EurJIC
European Journal of Inorganic Chemistry

Research Article
doi.org/10.1002/ejic.202300418

Chemistry Europe
European Chemical Societies Publishing

www.eurjic.org

Special Collection

How Ligand Geometry Affects the Reactivity of Co(II) Cyclam Complexes

Linda Iffland-Mühlhaus,[a] Beatrice Battistella,[b] Daniel Siegmund,[a, c] Kallol Ray,*[b] and Ulf-Peter Apfel*[a, c]

Cobalt complexes are extensively studied as bioinspired models for non-heme oxygenases as they facilitate both the stabilization and characterization of metal-oxygen intermediates. As an analog to the well-known Co(cyclam) complex **Co{N_4}** (cyclam = 1,4,8,11-tetraazacyclotetradecane), the Co^{II} complex **Co{i-N_4}** with the isomeric isocyclam ligand (isocyclam = 1,4,7,11-tetraazacyclotetradecane) was synthesized and characterized. Despite the identical N_4 donor set of both complexes, **Co{i-N_4}** enables the $2e^-/2H^+$ reduction of O_2 with a lower overpotential (η_{eff} of 385 mV vs. 540 mV for **Co{N_4}**), albeit with a diminished turnover frequency. Characterization of the intermediates formed upon O_2 activation of **Co{i-N_4}** reveals a structurally identified stable μ-peroxo Co^{III} dimer as the main product. A superoxo Co^{III} species is also formed as a minor product, as indicated by EPR spectroscopy. In further reactivity studies, the electrophilicity of these *in situ* generated Co–O_2 species was demonstrated by the oxidation of the O–H bond of TEMPO–H (2,2,6,6-tetramethylpiperidin-1-ol) *via* a H atom abstraction process. Unlike the known Co(cyclam), **Co{i-N_4}** can be employed in oxygen atom transfer reactions oxidizing triphenylphosphine to the corresponding phosphine oxide highlighting the impact of geometrical modifications of the ligand while preserving the ring size and donor atom set on the reactivity of biomimetic oxygen activating complexes.

Introduction

The activation of dioxygen (O_2) is essential for various biological and synthetic processes, like natural and artificial energy production (e.g. reduction of oxygen) or selective oxidation of organic molecules (e.g. alcohol and sulfur oxidation, C–H hydroxylation and alkene epoxidation).[1–6] In nature, O_2 activation is facilitated by heme and non-heme Fe and Cu metalloenzymes involving several reaction steps.[3,7–11] As a key step, metal-mediated binding of O_2 occurs to reduced Fe or Cu centers yielding highly reactive metal superoxo species,[12–14] which are subsequently converted to metal (hydro)peroxo and high-valent metal oxo species by further reduction and O–O bond cleavage steps. Such metal-O_2 intermediates have been intensively studied with a number of Fe and Cu transition metal complexes as biomimetic models.[12,15] Although of lower biological relevance compared to Fe and Cu, bioinspired Co based complexes have also gained attention as they possess a high affinity towards O_2 due to the higher thermodynamic and kinetic stability of Co^{III}–O_2 adducts formed from their corresponding Co^{II} precursors.[16] Accordingly, various Co–O_2 intermediates formed upon O_2 activation at Co centers are extensively studied for their application as catalysts for the selective oxidation of organic substrates as well as for oxygen reduction reactions (ORR).[17,22–27] Starting with the investigations of numerous heme-based Co complexes,[28–31] a tetradentate, nitrogen-rich coordination sphere represents a structural key feature for other O_2 activating non-heme Co complexes.[22,26,30,32–34] In particular, the O_2 activation capabilities of the Co complexes supported on cyclam-based macrocyclic motifs have been extensively investigated in the last two decades (Scheme 1).

For example, the reaction of the well-known Co(cyclam) complex **Co{N_4}** (cyclam = 1,4,8,11-tetraazacyclotetradecane) with O_2 in water has been demonstrated to yield either a 1:1 [Co^{III}–O_2] adduct or a μ-peroxo dimer $[Co_2(O_2)\{N_4\}]^{4+}$,[18] which are proposed as reactive intermediates formed during the electrochemical $2e^-/2H^+$ reduction of O_2 to hydrogen peroxide (H_2O_2).[18,19] Photocatalytic H_2O_2 production applying **Co{N_4}** as catalyst is also reported using semiconducting TiO_2 particles adsorbed on cellulose as photosensitizer.[35] Recently, we

[a] Dr. L. Iffland-Mühlhaus, Dr. D. Siegmund, Prof. Dr. U.-P. Apfel
Faculty of Chemistry and Biochemistry
Ruhr-Universität Bochum
Universitätsstraße 150
44780 Bochum (Germany)
E-mail: ulf.apfel@rub.de

[b] Dr. B. Battistella, Prof. Dr. K. Ray
Institut für Chemie
Humboldt-Universität zu Berlin
Brook-Taylor-Straße 2
12489 Berlin (Germany)
E-mail: kallol.ray@chemie.hu-berlin.de

[c] Dr. D. Siegmund, Prof. Dr. U.-P. Apfel
Department for Electrosynthesis
Fraunhofer Institute for Environmental Safety and Energy Technology
UMSICHT
Osterfelder Straße 3
46047 Oberhausen (Germany)

Supporting information for this article is available on the WWW under https://doi.org/10.1002/ejic.202300418

Special Collection Part of the Special Collection on "Inorganic Reaction Mechanisms". Part of the Wöhler Vereinigung für Anorganische Chemie Prize Winners Special Collection. Part of the Special Collection "Evolving with Inorganic Chemistry for 25 Years".

Research Article
doi.org/10.1002/ejic.202300418

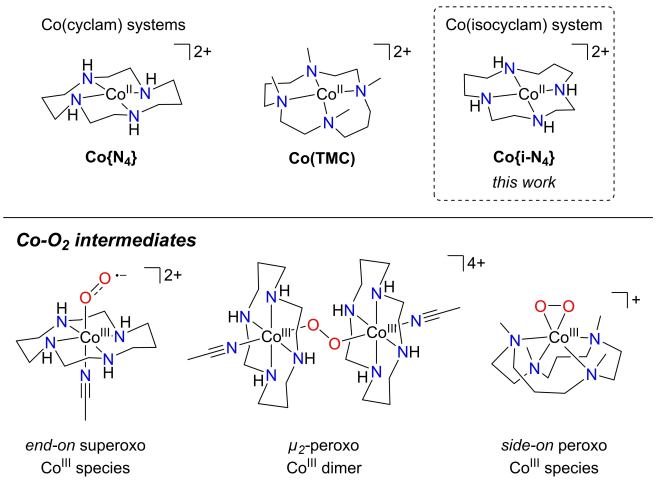

Scheme 1. 14-membered N_4 macrocyclic Co complexes for the activation and reduction of oxygen and their related Co–O_2 intermediates.[17–21]

reported the ORR capability of **Co{N_4}**, which was followed by UV/vis spectroscopy and simultaneously the turnover frequencies (TOF) and effective overpotentials (η_{eff}) determined as catalytic parameters for this reaction. Detailed spectroscopic studies further supported the formation of both mononuclear superoxo and dimeric peroxo species as Co–O_2 intermediates formed upon O_2 activation at **Co{N_4}**.[20] The generated Co–O_2 adducts based on the Co cyclam system were also investigated in oxidation reactions towards organic substrates. The peroxo complex, generated by the reaction of O_2 and **Co{N_4}**, was unreactive in oxygen atom transfer (OAT) reactions towards substrates like triphenylphosphine or SO_2.[36] However, the related hydroperoxo species $[Co(OOH)\{N_4\}]^{2+}$, generated by the chemical reduction of the superoxo species under acidic conditions, enables at least sulfur oxidation.[37] In addition, modification of the macrocyclic ligand by methylation of the N donor atoms leads to stabilization of a monomeric Co^{III} peroxo species formed upon addition of H_2O_2 in presence of a base; however the Co^{II}(TMC) complex (TMC = tetramethylated cyclam) is unable to react directly with O_2.[17,21] Similar complexes comprising methylated N_4 macrocyclic ligands with a different size were synthesized and characterized, whose molecular structures confirmed the presence of a *side-on* bound peroxo ligand.[38] Independent from the ligand ring-size, such metal-peroxo complexes facilitate aldehyde deformylation emphasizing the nucleophilic character known for Co-$\{O_2^{2-}\}$ intermediates.[21,38,39] In contrast, Co superoxo intermediates exhibit electrophilic character enabling C–H and O–H bond activations in hydrogen atom transfer (HAT) or reacting in OAT reactions.[25,27,40] Thus, Co–O_2 adducts are of interest not only as key intermediates in the field of catalytic oxygen reduction but can also be relevant in the catalysis of many other oxidative reactions. Within this context, the redox potential of the $Co^{III/II}$ couple plays a crucial role for the performance of the related compounds. Since the modification of the ligand framework strongly affects the $Co^{III/II}$ redox potential, both the reactivity towards O_2 and the catalytic activity in ORR can be influenced, as shown for a series of Co porphyrin and pseudo-macrocyclic ketiiminate complexes.[18,29] Considering cyclam-based systems, it was shown that substitution or exchange of N donor atoms by chalcogens affects the electrochemical properties of the metal center.[41–48] However, geometrical modification while maintaining the ring size and donor set of the macrocyclic ligand can lead to altered metal-related reduction/oxidation potentials as shown for Ni, Cu and Re complexes comprising isocyclam (1,4,7,12-tetraazacyclotetradecane, **{i-N_4}**) as ligand.[44,49,50] For those complexes the redox potentials of $Ni^{II/I}$, $Cu^{III/II}$ and $Cu^{II/I}$, as well as $Re^{I/0}$ were shifted to milder potentials by utilizing **{i-N_4}** as ligand instead of cyclam **{N_4}**. A similar trend was also reported for the $Co^{III/II}$ redox potential of the Co analogs in polarographic studies with various macrocyclic complexes.[51] However, the isocyclam Co complex **Co{i-N_4}** was never structurally described or further characterized in detail. Inspired by the reactivity of $[Co(cyclam)]^{2+}$ towards O_2, we became interested in which extent a structural alteration of the ligand scaffold can affect the Co–O_2 interaction in **Co{i-N_4}**. Thus, we herein report the synthesis of **Co{i-N_4}**, its structural and electrochemical properties and investigate its reactivity towards oxygen, and the catalytic potential in the oxygen reduction reaction, as well as in other oxidative processes such as HAT and OAT reactions.

Results and Discussion

Synthesis and characterization

The isocyclam ligand **{i-N_4}** was prepared according to the literature described procedure,[43] while its complexation was performed by the addition of an equimolar amount of Co-$(ClO_4)_2 \cdot 6H_2O$ in acetonitrile under Ar atmosphere. Purification was conducted *via* column chromatography with acetonitrile as eluent affording compound **Co{i-N_4}** as a red solid in 72% yield. Complex formation was supported by ESI mass spectrometry revealing a characteristic mass peak at $m/z = 358.0$ assigned to the $[Co\{i\text{-}N_4\}(ClO_4)]^+$ fragment and showing the expected isotopic pattern (Figure S1). The IR spectrum of the isolated solid exhibits two characteristic C≡N stretching frequencies at 2297 and 2261 cm^{-1} suggesting an additional coordination of acetonitrile to the Co center (Figure S2). This assumption was further confirmed by analysis of the molecular structure *via* X-ray diffraction (XRD) analysis using single-crystals grown from an acetonitrile solution of **Co{i-N_4}** *via* vapor diffusion of diethyl ether at −35 °C. Similar to the Co(cyclam) complex,[42] the Co^{II} center in **Co{i-N_4}** exhibits an octahedral geometry. Herein the four donor atoms of the macrocyclic ligand are bound in a planar fashion, while two additional acetonitrile molecules complete the octahedral coordination sphere in the axial positions (Figure 1, Table S1). UV/vis spectrum of **Co{i-N_4}** in acetonitrile showed a defined absorption maximum at a wavelength of 479 nm ($\varepsilon = 135\ M^{-1}cm^{-1}$) with an additional shoulder at around 564 nm ($\varepsilon = 51\ M^{-1}cm^{-1}$) (Figure 2, S3), as known for other octahedral Co^{II} complexes bearing a tetradentate macrocyclic ligand.[52] The corresponding solid-state UV/vis spectrum

Research Article
doi.org/10.1002/ejic.202300418

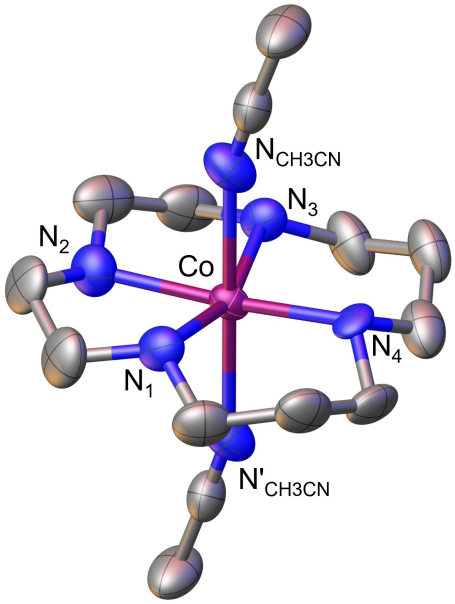

Figure 1. XRD determined molecular structure of **Co{i-N_4}** with thermal ellipsoids drawn at 50% probability level. Hydrogen atoms and perchlorate counter ions are omitted for clarity. Gray: carbon, blue: nitrogen, purple: cobalt.[57]

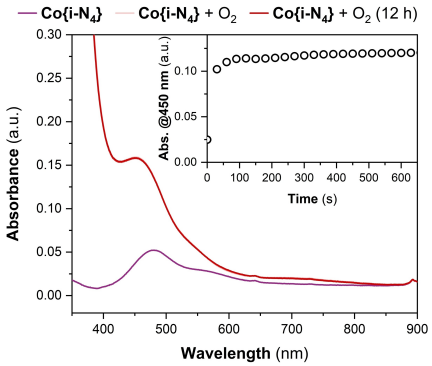

Figure 2. UV/vis spectra of **Co{i-N_4}** (0.5 mM) in acetonitrile (purple) and after addition of O_2 (red). Inset: Change in absorption at 450 nm over time after addition of O_2.

of the complex features a similar absorption pattern indicating that the molecular structure obtained by XRD is maintained in solution and the octahedral coordination sphere of the Co^{II} center is preserved (Figure S3). The magnetic moment of **Co{i-N_4}** in a deuterated acetonitrile solution was first measured by Evans method,[53–56] giving rise to $\mu_{eff} = 1.60\ \mu_B$. This value is in line with a theoretical spin-only value of 1.73 μ_B expected for a $S = 1/2$ system. The X-band EPR spectrum of **Co{i-N_4}** in acetonitrile at 13 K exhibits signals at effective $g = 4.98$, 2.26 and 1.98 (Figure S4). These EPR features find the best fit considering the merged contribution of a predominant low spin Co^{II} species with $S = 1/2$ ($g_\perp = 2.24$ and $g_\parallel = 1.98$, 86%), and a minor high spin Co^{II} species with $S = 3/2$ ($g_\perp = 4.98$, $g_\parallel = 2.28$, 11%). **Co{i-N_4}** was further characterized by cyclic voltammetry (CV) in dry acetonitrile containing 0.1 M tetrabutylammonium hexafluorophosphate ($[^nBu_4N]PF_6$) as supporting electrolyte (Figure 3, Table 1). The obtained CV reveals similar reduction and oxidation processes as observed for **Co{N_4}** (Table 1). Based on the reported CV of **Co{N_4}**, the reductive signal at −2.01 V vs. $Fc^{+/0}$ for **Co{i-N_4}** can be attributed to the reduction of Co^{II} to Co^{I}.[42,58] The reoxidation of Co^{I} to Co^{II} occurs at −1.89 V vs. $Fc^{+/0}$ with a depleted intensity (i_{pc}/i_{pa} ratio of 0.35), which may suggest an irreversible process (Figure S5). The second reduction signal at potentials more negative than −2.6 V vs. $Fc^{+/0}$ can be assigned to the irreversible $Co^{I/0}$ reduction. The additional quasi-reversible redox signal with $E_{1/2}$ at 0.12 V vs. $Fc^{+/0}$ corresponds to the $Co^{III/II}$ redox couple. Although a peak-to-peak separation of $\Delta E_p = 550$ mV is observed for the $Co^{III/II}$ redox couple, scan-rate dependent studies reveal a value of 0.97 for the i_{pc}/i_{pa} ratio confirming the high reversibility of this redox process (Figure S6). While the $Co^{II/I}$ reduction and the $Co^{III/II}$ redox potentials are less affected by the altered ligand geometry, for **Co{i-N_4}** a large cathodic shift (> 400 mV) is observed for the $Co^{I/0}$ potential compared to **Co{N_4}** (Table 1).

ORR capability and reactivity towards O_2

Inspired by the reactivity of the reported Co cyclam analog towards O_2, the ORR capability of **Co{i-N_4}** was investigated by UV/vis spectroscopy. Even in the presence of a weak electron donor like ferrocene (Fc, $E_{ox} = 0.37$ V vs. SCE)[59] using trifluoroacetic acid (TFA) as a proton source, **Co{i-N_4}** enables the catalytic reduction of O_2. The reaction was monitored by the rise in absorbance at 619 nm, which verifies the formation of the ferrocenium cation (Fc^+) (Figure 4).[60,61] Notably, in absence

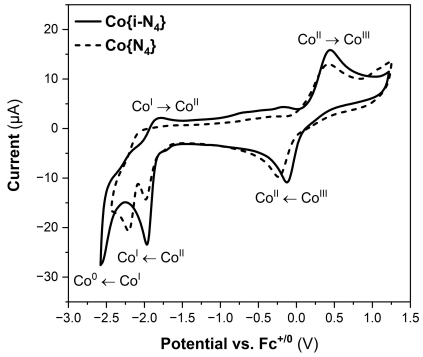

Figure 3. Cyclic voltammogram of **Co{i-N_4}** (1 mM) compared to **Co{N_4}** (CV adapted from ref. [42]) in acetonitrile with 0.1 M tetrabutylammonium hexafluorophosphate ($[^nBu_4N]PF_6$) as supporting electrolyte.

Table 1. Potentials for the metal-related reduction and oxidation processes of **Co{i-N_4}** (1 mM) in acetonitrile with $[^nBu_4N]PF_6$ (0.1 M) compared to the cyclam derivative **Co{N_4}**.[42]

Reduction/oxidation process	**Co{i-N_4}** (V vs. $Fc^{+/0}$)	**Co{N_4}**[42] (V vs. $Fc^{+/0}$)
$E_{pc}(Co^{II/I})$	−2.01	-1.98
$E_{pc}(Co^{I/0})$	< −2.60	-2.21
$E_{1/2}(Co^{III/II})$	0.12	0.09

Research Article
doi.org/10.1002/ejic.202300418

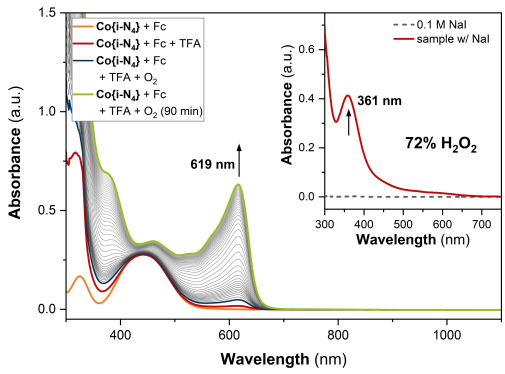

Figure 4. UV/vis spectral changes observed in the oxygen reduction reaction using **Co{i-N$_4$}** (0.1 mM) with ferrocene as one-electron donor (3 mM) and trifluoroacetic acid as proton source (10 mM) in O_2-saturated acetonitrile (12.1 mM)[64] at RT. Inset: Iodometric titration performed on an aliquot (0.02 mL) of the final reaction mixture confirmed H_2O_2 formation (see SI for further information).

of **Co{i-N$_4$}** no Fc^+ formation and thus no reduction of O_2 was detected by UV/vis spectroscopy (Figure S7). Oxygen reduction can either proceed *via* a $2e^-/2H^+$ reduction forming H_2O_2 or *via* a $4e^-/4H^+$ pathway yielding water (Equation 1 and 2). In the case of **Co{i-N$_4$}** catalyzed ORR, iodometric titration[59] of the final reaction mixture showed the formation of H_2O_2 in 72% yield (Inset Figure 3, see SI for further information).

$$O_2 + 2\ e^- + 2H^+ \rightarrow H_2O_2 \qquad E^O = 0.68\ V\ vs.\ NHE \qquad (1)$$

$$O_2 + 4\ e^- + 4H^+ \rightarrow 2\ H_2O \qquad E^O = 1.23\ V\ vs.\ NHE \qquad (2)$$

Nevertheless, due to the instability of the formed ferrocenium cation,[62] decamethylferrocene (Fc*, $E_{ox} = -0.08$ V vs. SCE)[59] was used as a reductant for further mechanistic investigations. Thereby ORR can be monitored at 778 nm as it is the characteristic absorbance band for the stable decamethylferrocenium cation (Fc^{*+}) (Figure S8A).[61] Similar to the catalytic reaction using Fc as a reductant, oxygen titration experiments confirmed the formation of H_2O_2 by a ratio of 2.17 ± 0.09 between the applied oxygen concentration and the concentration of Fc^{*+} (Figure S9, see SI for further information). Moreover, iodometric titration showed H_2O_2 production in high selectivity (94%) (Figure S8B). To exclude that the catalytic activity is due to free Co^{2+} ions potentially formed by complex degradation, a control experiment using a Co^{II} salt as a catalyst was performed (Figure S10A). In addition, a control experiment in the absence of any catalyst was carried out as well, since Fc* is also known to enable the reduction of O_2 (Figure S10B).[63] However, both control experiments showed a significantly lower reactivity compared to the **Co{i-N$_4$}** catalyzed reaction (Figure S11). For evaluation of the catalytic potential, the turnover frequency (TOF) of the O_2 to H_2O_2 conversion was determined under buffered conditions (TFA and sodium trifluoroacetate, NaTFA) using the initial rates of Fc^{*+} formation ($d[Fc^{*+}]/dt$) obtained by UV/vis spectroscopy (see SI for further information). Considering the concentration of **Co{i-N$_4$}** used as the catalyst, a TOF of $6.43 \cdot 10^{-2}$ s^{-1} was determined for the ORR, which is lower by half compared to the TOF reported for the cyclam-derivative **Co{N$_4$}** (0.124 s^{-1}).[20] For further analysis of the catalytic performance, the effective overpotential (η_{eff}), defined as the difference between the thermodynamic potential ($E_{O2/H2O2}$) for the O_2 to H_2O_2 reduction and the redox potential $E_{1/2}(Co^{III/II})$ of the Co complex under buffered conditions, was considered. For **Co{i-N$_4$}**, upon addition of TFA and NaTFA (10 mM each), the redox potential of the $Co^{III/II}$ couple is cathodically shifted to −0.34 V vs. $Fc^{0/+}$ ($\Delta E = 461$ mV) (Figure S14) probably caused by exchange and coordination of the counterions by trifluoroacetate. Similar behavior has already been reported for **Co{N$_4$}** and its sulfur-substituted analog.[20] Additional UV/vis studies following the reaction of **Co{i-N$_4$}** with an excess of sodium triflate (10 equiv.) show a direct change of the absorption pattern (Figure S15) suggesting the coordination of trifluoroacetate to the metal center and an associated switch in the ligand configuration from a planar to a folded geometry as reported for the sulfur-substituted Co cyclam derivative.[20] Contrary to **Co{i-N$_4$}**, the UV/vis spectra of **Co{N$_4$}** did not show a significant change in the absorbance indicating that a planar coordination geometry of the ligand is maintained even in the presence of trifluoroacetate. The higher affinity of **Co{i-N$_4$}** to change the ligand binding mode, can be reasonably explained by the bond length in both complexes. While for **Co{N$_4$}** the distances between the Co^{II} ion and the N atoms of the macrocyclic ligand are nearly identical (1.9978(18) and 2.0012(18) Å),[1] in **Co{i-N$_4$}** the Co–N bond lengths vary in a range of 1.95(2) to 2.07(3) Å. The latter implies that the Co^{II} ion fits less perfectly in the cavity of the isocyclam macrocycle, favoring a conformational change of the ligand. Furthermore, a slightly elongated distance between the Co center and the coordinated acetonitrile ligand indicates a weaker bond ($Co–N_{MeCN}$: 2.237(6) Å for **Co{i-N$_4$}** and 2.229(2) Å for **Co{N$_4$}**[1]), which promotes a ligand exchange and a concomitant coordination change.

Due to the different coordination behavior of both complexes in presence of additional anions, the potential shift between non-catalytic (pure acetonitrile) and catalytic (acetonitrile with TFA and NaTFA, 10 mM each) conditions is comparably smaller for **Co{i-N$_4$}** than for **Co{N$_4$}**. Considering the thermodynamic potential $E_{O2/H2O2}$ under non-aqueous conditions determined by open-circuit potential (OCP) measurements for $E_{H+/H2}$ following a reported methodology (see SI for further information),[20,65,66] the more anodic $Co^{(III/II}$ redox potential of **Co{i-N$_4$}** results in a lower η_{eff} value of 385 mV compared to **Co{N$_4$}** (541 mV),[20] demonstrating the beneficial influence of the geometrical alternation of the ligand on the O_2 reduction reaction.

In addition to the spectrochemical approach using a chemical reductant (Fc or Fc*), the electrons for ORR can alternatively be provided electrochemically. Thus, electrochemical studies using **Co{i-N$_4$}** as a catalyst were performed under similar reaction conditions as used for the spectrochemical investigation in the absence of the chemical one-electron reductant. As supported by control experiments in the absence

Research Article
doi.org/10.1002/ejic.202300418

of **Co{i-N$_4$}**, the uncatalyzed oxygen reduction starts in the presence of TFA (10 mM) at a potential of around −0.46 V vs. $Fc^{+/0}$ (Figure S18). In the presence of **Co{i-N$_4$}** (1 mM) the catalytic current already starts at a potential around 0 V vs. $Fc^{+/0}$, while in presence of the isomeric **Co{N$_4$}** (1 mM) analog increase of the catalytic current is observed around −0.14 V vs. $Fc^{+/0}$. Comparing the observed potentials at −0.1 mA, **Co{i-N$_4$}** enables the reduction of O_2 at a 210 mV milder potential as **Co{N$_4$}** and a 300 mV positively shifted potential as compared to the measurement without any Co complex.

The reaction of **Co{i-N$_4$}** with O_2 leads to an immediate color change from red to orange, which can be also followed by UV/vis spectroscopy. The characteristic absorption band of **Co{i-N$_4$}** at 479 nm is shifted to 450 nm and an additional shoulder at around 535 nm together with a concomitant rise in absorbance at 710 nm takes place (Figure 2A). The newly formed species **Co{i-N$_4$}–O$_2$** is stable for more than 12 h at RT as could be proven by UV/vis spectroscopy (Figure 2A Inset). For the cyclam-derivative **Co{N$_4$}**, a superoxo Co^{III} and a dimeric μ-peroxo Co^{III} species were reported as reactive intermediates.[20] To identify the Co–O_2 species present in **Co{i-N$_4$}–O$_2$**, X-band EPR spectrum of a solution of **Co{i-N$_4$}** after exposure to O_2 was recorded at 13 K (Figure 5B). Simulation of the experimental EPR features reveals the presence of two species. The signal with effective $g_\perp = 2.10$ and $g_\parallel = 2.00$ points to the formation of a $[Co^{III}(O_2^{\bullet})]^{2+}$ species resembling EPR parameters of previously reported Co^{III} superoxo species.[20,25–27,40,67] The other species with effective $g_\perp = 4.73$ and $g_\parallel = 2.26$ could be assigned to an additional unidentified $S = 3/2$ Co^{II} species. XRD analysis of crystals grown from a high concentrated **Co{i-N$_4$}** acetonitrile solution at room temperature after exposure to air confirmed formation of a peroxo-bridged dimer **Co$_2$(O$_2$){i-N$_4$}$_2$** (Figure 5C) as an additional diamagnetic Co–O_2 intermediate. The bridging μ_2-peroxo binding mode is commonly observed in Cu containing enzymes known for their O_2 activation capability,[68,69] as well as in biomimetic synthetic Cu and Co complexes.[25,26,70–72] In the herein received structure of **Co$_2$(O$_2$){i-N$_4$}$_2$** each Co^{III} atom is coordinated in-plane by the four N-donor atoms of one macrocyclic ligand and axially by the bound μ-peroxo and acetonitrile ligands. Similar coordination behavior was postulated for the cyclam-based Co complex and structurally proven for a sulfur-containing cyclam-analog.[20] Notably, the Co–O distance of 1.8930(17) Å as well as the O–O distance of 1.442(5) Å (Table S3) are in line with the ones reported for other pentaamine Co^{III}–O_2 complexes.[26,73,74] Moreover, X-band EPR analysis in perpendicular mode of solid **Co$_2$O$_2${i-N$_4$}$_2$** gave no signal as expected and the spectrum of the re-dissolved complex (1 mM) exclude reversible interconversion between the different Co–O_2 species, since the $S = 1/2$ signal ascribable to $[Co^{III}(O_2^{\bullet})]^{2+}$ was present only in 1% (0.01 mM) yield (Figure S19). These results are in line with the UV/vis spectra of **Co$_2$(O$_2$){i-N$_4$}$_2$** in solid-state and in acetonitrile solution (Figure S20). These findings also suggest that **Co$_2$(O$_2$){i-N$_4$}$_2$** is formed as a main species from the reaction of **Co{i-N$_4$}** with O_2 and are in line with previous studies on the cyclam derivative **Co{N$_4$}** which described that different Co–O_2 species are formed depending on the Co complex/O_2 ratio.[18]

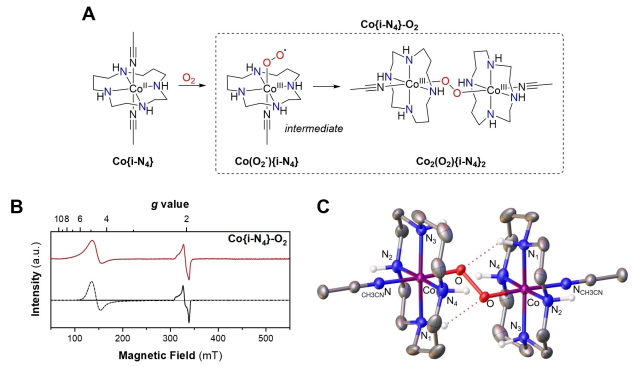

Figure 5. (A) Reactivity of **Co{i-N$_4$}** towards O_2. (B) X-band EPR spectrum of **Co{i-N$_4$}–O$_2$** (1 mM) in acetonitrile measured at 13 K, 9.35 GHz, 1 mW (red) and the corresponding simulated spectrum (grey). (C) XRD determined molecular structure of the μperoxo bridged dimer **Co$_2$(O$_2$){i-N$_4$}$_2$** with thermal ellipsoids drawn at 50% probability level. Hydrogen atoms, except of those bound to nitrogen, and perchlorate counter ions are omitted for clarity. Gray: carbon, blue: nitrogen, red: oxygen, purple: cobalt.[57]

Substrate oxidation reactivity

Co–O_2 species are also known for their reactivity towards organic substrates in electrophilic and/or nucleophilic oxidation reactions like HAT, OAT or aldehyde deformylation reactions.[25,27,39,40] To investigate the chemical properties of the *in situ* generated Co–O_2 intermediates **Co{i-N$_4$}–O$_2$**, an O_2-saturated solution of **Co{i-N$_4$}** was reacted with organic substrates and the spectral changes were followed by UV/vis spectroscopy. The reaction of **Co{i-N$_4$}–O$_2$** with one equivalent 2,2,6,6-tetramethylpiperidin-1-ol (TEMPO–H) as a hydrogen atom donor at RT results in the disappearance of the absorption band at 710 nm and formation of a new band at around 570 nm. Likewise, absorption around 450 nm decreased and the maximum shifted to 465 nm (Figure S21). Furthermore, X-band EPR spectrum of a reaction solution of **Co{i-N$_4$}–O$_2$** with one equivalent TEMPO-H after air exposure shows an intense $S = 1/2$ signal with effective $g = 2.00$ ascribable to the TEMPO$^{\bullet}$ radical formed by H-abstraction (Figure S22). Quantification of the EPR spectrum using a 1 mM Cu^{II} standard confirmed 87% conversion of TEMPO–H to TEMPO$^{\bullet}$. This result suggests that only the low-spin Co^{II} species of **Co{i-N$_4$}** (86%) reacts with O_2, and both intermediates in **Co{i-N$_4$}–O$_2$** are capable to abstract a H atom from the organic substrate. For comparison, the reaction of the isolated μ-peroxo dimer **Co$_2$(O$_2$){i-N$_4$}$_2$** with TEMPO–H was investigated separately showing similar spectral changes, although the reaction proceeds slower in comparison to the *in situ* generated species **Co{i-N$_4$}–O$_2$** (Figure S21). During the H-abstraction, the reactive Co–O_2 species are presumably converted into a Co^{III} hydroperoxo species. In order to verify this suggestion, a hydroperoxo species was generated using a literature described procedure and investigated by UV/vis spectroscopy.[75] Within these UV/vis experiments, **Co{i-N$_4$}** was reacted first with 10 equiv. H_2O_2 or urea·H_2O_2 in presence of 2 equiv. triethylamine to form a peroxo species which was then converted into the corresponding hydroperoxo species by the

Research Article
doi.org/10.1002/ejic.202300418

addition of 3 equiv. perchloric acid. The recorded UV/vis spectra from these reaction solutions were then compared to the obtained spectrum from the reaction of **Co{i-N$_4$}–O$_2$** with TEMPO–H (Figure S23), showing similar absorption bands and thus indicating formation of a hydroperoxo species. Since TEMPO–H is a comparably mild O–H substrate indicated by its O–H bond dissociation energy (BDE) of 70.6 kcal mol^{-1} in acetonitrile,[76] the O–H bond in TEMPO–H can be easily oxidized. Further HAT from O–H bonds by **Co{i-N$_4$}–O$_2$** was performed using 2,4,6-tri-*tert*-butylphenol (2,4,6-TTBP) with a stronger O–H bond (BDE = 81.6 kcal mol^{-1} in acetonitrile).[76] Addition of an excess of 2,4,6-TTBP results in similar spectral changes as the reaction with TEMPO–H (Figure S24) indicating the formation of the same hydroperoxo Co species. Gas chromatography-mass spectrometry (GC-MS) of the reaction mixture proves the presence of a small amount 2,6-di-*tert*-butyl-1,4-benzoquinone known to be formed after oxidation of 2,4,6-TTBP to the phenoxy radical (Figure S25).[77] Due to the low substrate conversion, the substrate amount was reduced using only one equivalent 2,4,6-TTBP. After 24 h the corresponding UV/vis spectrum indicated complete conversion since spectral changes were no longer observed. However, the corresponding gas chromatogram of the reaction mixture shows an intense signal for non-converted starting material and 2,6-di-*tert*-butyl-1,4-benzoquinone to a less extent only (Figure S26). Nevertheless, the formation of 2,6-di-*tert*-butyl-1,4-benzoquinone is ascribable to the presence of the Co–O$_2$ intermediates as proven by a control experiment without any Co complex (Figure S26). Moreover, the related X-band EPR spectrum of an aliquot of the reaction mixture shows an additional signal at $g = 2.00$, ascribable to the formation of the corresponding phenoxy radical, but also the typical signals of **Co{i-N$_4$}–O$_2$** (Figure S27). The resulting suggestion that the EPR-silent μ-peroxo dimer promotes the HAT reaction, was further supported by a UV/vis experiment employing isolated **Co$_2$(O$_2$){i-N$_4$}$_2$** (Figure S24). Similar results as obtained for the reactivity towards 2,4,6-TTBP were observed employing **Co{i-N$_4$}–O$_2$** in C–H bond activation using xanthene (BDE = 75.5 kcal mol^{-1})[78] and 1,4-cyclohexadiene (1,4-CHD, BDE = 76.0 kcal mol^{-1})[79] as organic substrates (Figure S28 and S29).

Reactivity properties of the **Co{i-N$_4$}–O$_2$** intermediates were further studied in OAT reactions using thioanisole and triphenylphosphine (PPh$_3$) as organic substrates. Following the reaction with thioanisole by UV/vis spectroscopy and subsequent analysis of the reaction mixture *via* GC-MS proved **Co{i-N$_4$}–O$_2$** to be unreactive in sulfoxidation reaction (Figure S30). In contrast, UV/vis spectra monitoring the reaction with PPh$_3$ (50 equiv.) show first a decrease in absorbance at 450 nm followed by an increase suggesting an initial consumption and subsequent recovery of **Co{i-N$_4$}–O$_2$** (Figure S31A). Analysis of the reaction solution by ^{1}H and ^{31}P NMR spectroscopy showed complete conversion of PPh$_3$ (^{1}H NMR: δ (ppm) = 7.35 (m) and 7.27 (m), ^{31}P NMR: δ (ppm) = -5.1) to triphenylphosphine oxide (OPPh$_3$; ^{1}H NMR: δ (ppm) = 7.61 (m) and 7.49 (m), ^{31}P NMR: δ (ppm) = 26.7), which was further confirmed by GC-MS analysis (Figure 6A, 6B and S31B). For the reaction using 2 mol% of **Co{i-N$_4$}** in the presence of O$_2$ a turnover frequency (TOF) of 14.4 h^{-1} was determined from time-dependent ^{31}P NMR spectroscopic product analysis (Figure 6C and S32). Control experiments under an inert atmosphere and without **Co{i-N$_4$}** verified that oxidation of PPh$_3$ is indeed catalyzed by the *in situ* formed Co–O$_2$ species (Figure 6A, 6B and S31B). Remarkably, the isolated μ-peroxo dimer **Co$_2$(O$_2$){i-N$_4$}$_2$** also oxidize PPh$_3$ (Figure S33) forming the corresponding oxide in stoichiometric yield. Notably, Co(III)-peroxo mediated electrophilic OAT reactions are extremely rare in the literature.[80] Moreover, this experiment confirmed the regeneration of the active species after complete conversion since the catalytic reaction could be restarted by the addition of new substrate (Figure S33) in the presence of excess oxygen. The reactivity of the *in situ* generated Co–O$_2$ species of **Co{i-N$_4$}** towards aldehydes was also studied, since (hydro)peroxide Co complexes are frequently known to allow the deformylation reaction of aldehydes, emphasizing their nucleophilic character.[21,38,39] However, **Co{i-N$_4$}–O$_2$** was shown to be unreactive towards 2-phenylpropionaldehyde (2-PPA) and no acetophenone as the expected deformylation product was detected by GC-MS (Figure S34).

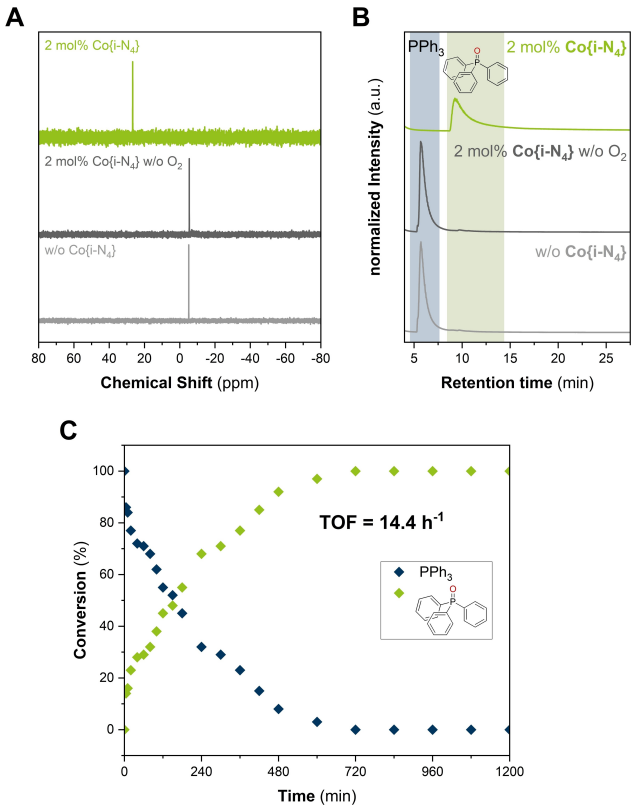

Figure 6. (A) ^{31}P NMR spectra for the oxidation of PPh$_3$ catalyzed by 2 mol% **Co{i-N$_4$}** in presence of air, and for the corresponding control experiments under exclusion of air and without Co catalyst. (B) Gas chromatograms from GC-MS analysis of the oxidation of PPh$_3$ catalyzed by 2 mol% **Co{i-N$_4$}** in presence of air, and for the corresponding control experiments under exclusion of air and without Co catalyst. (C) Time-dependent conversion of PPh$_3$ to OPPh$_3$ catalyzed by 2 mol% **Co{i-N$_4$}** in presence of air based on ^{13}P NMR spectroscopic analysis (Figure S31).

Research Article
doi.org/10.1002/ejic.202300418

Conclusions

In summary, the synthesis and characterization of isocyclam-ligated Co^{II} complex **Co{i-N$_4$}** was described. Similar to the cyclam derivative **Co{N$_4$}**, **Co{i-N$_4$}** applied as a homogenous catalyst in ORR was shown to facilitate the O_2 reduction *via* a $2e^-/2H^+$ pathway yielding H_2O_2 in high selectivity. However, for **Co{i-N$_4$}** an effective overpotential n_{eff} of 385 mV was determined, which is around 150 mV lower than n_{eff} of **Co{N$_4$}** under identical reaction conditions due to their different anion exchange behavior. As reactive Co–O_2 species generated at RT in a direct reaction with O_2 both a mononuclear superoxo Co^{III} intermediate and a structurally characterized dimeric μ-peroxo Co^{III} complex **Co$_2$(O$_2$){i-N$_4$}$_2$** were confirmed. In contrast to literature reported **Co{N$_4$}**,[36] the *in situ* generated Co–O_2 species of **Co{i-N$_4$}** were shown to react as oxidants in electrophilic oxidation reactions towards external substrates. While for HAT reactions only a low reactivity was detected, strongly depending on the BDE of the respective substrate, the Co–O_2 intermediate was shown to be highly reactive in OAT, catalytically oxidizing PPh_3 to $OPPh_3$ with a TOF of 14.4 h^{-1}. Since the Co cyclam analog was reported to be unreactive in OAT, this finding demonstrates how small adaptions of the ligand and concomitant slight changes in the coordination of the metal center led to a higher stabilization of reactive intermediates and a significantly altered reactivity of such macrocyclic Co complexes.

Experimental Section

General considerations

Complexation reactions were performed under a dry Ar atmosphere by working in a *MBraun* UNIlab^{ECO} glovebox. Starting materials and chemicals were obtained from commercial suppliers and used without further purification. All used solvents were dried by a *MBraun* SPS solvent purification system or according to standard methods.[81] Isocyclam **{i-N$_4$}** was synthesized according to the literature known procedure.[43] ^{1}H NMR and ^{31}P spectra were recorded with a *Bruker* AVIII-400 NMR spectrometer and are reported in parts per million (ppm). ^{1}H NMR spectra are referenced to residual solvent signals, while ^{31}P NMR spectra are referenced using 85% H_3PO_4 as external standard. ESI mass spectra were obtained with a *Bruker* Daltonics Esquire 6000 instrument. IR spectra were recorded with a *Shimadzu* IRTracer-100 attached to a Pike Miracle ATR unit and are reported in cm^{-1}. UV/vis spectra were recorded with a *Shimadzu* UV-1900i UV/vis spectrophotometer and are reported in nm. EPR spectra were recorded on a *Bruker* EMXplus X-band spectrometer with a microwave frequency amounted to around 9.35 GHz. All samples were measured as frozen solutions or solids at 13 K using a liquid helium recirculation cooling system provided by *ColdEdge*. EPR spectral simulations were performed using the *EasySpin* software version 5.2.35 supported by MATLAB.[82] CHN elemental analyses were measured with an *Elementar* vario MICRO cube. Gas chromatography-mass spectrometry (GC-MS) analyses were performed using a *Shimadzu* GCMS-QP2010 Plus system equipped with a capillary column and a MS detector. Liquid phase separation was performed *via* hand-injection using a FS-OV-1-CB dimethylsilicone capillary GC column (L×I.D. 25 m×0.25 mm, average thickness 0.25 μm). Helium was used as a carrier gas. The electrochemical studies were performed using a PalmSens3 or PalmSens4 potentiostat in a three-electrode setup including a glassy carbon working electrode, a Pt wire counter electrode and a Ag wire as pseudoreference electrode. The working electrode was prepared by successive polishing and subsequent sonication in the applied solvent for 10 min prior to its use. Tetrabutylammonium hexafluorophosphate (0.1 M, [^{n}Bu$_4$N]PF_6) was used in organic media as supporting electrolyte. If not otherwise mentioned, all experiments were performed under an inert Ar atmosphere and all pseudoreferenced potentials were afterwards referenced against the ferrocene/ferrocenium redox potential ($Fc^{+/0}$). Further detailed information about the performed experiments for H_2O_2 identification and quantification and spectrochemical oxygen reduction reaction, as well as information about open-circuit potential (OCP) measurements and CV experiments are described in the Supporting Information (SI).

Caution! Perchlorate salts of metal complexes are potentially explosive. They should be handled with care and prepared only in small quantities.

Synthesis

[Co{i-N$_4$}(CH$_3$CN)$_2$](ClO$_4$)$_2$ (Co{i-N$_4$}). Compound {i-N$_4$} (100 mg, 0.5 mmol) was suspended in 3 mL acetonitrile and a solution of $Co(ClO_4)_2 \cdot 6H_2O$ (183 mg, 0.5 mmol) in 3 mL acetonitrile was added dropwise. After the complete addition of the Co salt solution, the reaction mixture was stirred for further 12 h at room temperature. The reaction mixture was filtered, and the obtained solution was layered with diethyl ether. The formed solid was separated, washed with additional diethyl ether, and dried under reduced pressure. The obtained solid was purified by filtration over a short silica column with acetonitrile as eluent. Compound **Co{i-N$_4$}** (194 mg, 0.36 mmol) was obtained as a red solid in 72% yield. Crystals suitable for X-ray diffraction analysis were grown from an acetonitrile solution by diethyl ether diffusion at −35 °C. ESI MS: calcd for $[C_{10}H_{24}ClCoN_4O_4]^+$ and $[C_{10}H_{23}CoN_4]^+$: m/z = 358.1 and 258.1, found: m/z = 358.0 and 258.6. IR (ATR): $\tilde{\nu}$ = 930, 995, 1018, 1055, 1086, 1425, 1472, 2264, 2332, 2359, 2884, 2941, 3240 cm^{-1}. UV/vis (CH_3CN): λ_{max} = 479 nm (ε = 135 $L\,mol^{-1}\,cm^{-1}$), 564 nm (ε = 51 $L\,mol^{-1}\,cm^{-1}$).

[Co$_2$(O$_2$){i-N$_4$}$_2$(CH$_3$CN)$_2$](ClO$_4$)$_4$ (Co$_2$(O$_2$){i-N$_4$}$_2$): In the presence of air, a highly concentrated acetonitrile solution of **Co{i-N$_4$}** was reacted with dioxygen forming compound **Co$_2$(O$_2$){i-N$_4$}$_2$** as an orange solid. Crystals suitable for X-ray diffraction analysis were directly obtained from acetonitrile solutions. IR (ATR): $\tilde{\nu}$ = 851, 887, 934, 974, 1030, 1059, 1090, 1429, 1449, 1477, 2259, 2303, 2893, 2926, 2963, 3223 cm^{-1}. Anal. calcd for $[C_{25}H_{54}Cl_4Co_2N_{10}O_{18}]$: C 27.98, H 5.28, N 13.59. Found: C 28.03, H 5.152, N 13.60.

Supporting Information

The authors have cited additional references within the Supporting Information.[22–24,83–90]

Acknowledgements

We thank the Deutsche Forschungsgemeinschaft (DFG, German Research Foundation) for financial support under Germany's Excellence Strategy – EXC 2033 – 390677874 – RESOLV, AP242/5-1 and RA/2409/8-1. This work was further supported by the

Fraunhofer Internal Programs under Grant no. Attract 097-602175. Open Access funding enabled and organized by Projekt DEAL.

Conflict of Interests

The authors declare no conflict of interest.

Data Availability Statement

The data that support the findings of this study are available from the corresponding author upon reasonable request.

Keywords: O–O activation · cobalt · macrocyclic ligands · ligand effects · reaction mechanisms

[1] L. Que, *JBIC J. Biol. Inorg. Chem.* **2017**, *22*, 171–173.
[2] E. G. Kovaleva, J. D. Lipscomb, *Nat. Chem. Biol.* **2008**, *4*, 186–193.
[3] M. Guo, T. Corona, K. Ray, W. Nam, *ACS Cent. Sci.* **2019**, *5*, 13–28.
[4] D. Wang, A. B. Weinstein, P. B. White, S. S. Stahl, *Chem. Rev.* **2018**, *118*, 2636–2679.
[5] A. N. Campbell, S. S. Stahl, *Acc. Chem. Res.* **2012**, *45*, 851–863.
[6] M. Shao, Q. Chang, J.-P. Dodelet, R. Chenitz, *Chem. Rev.* **2016**, *116*, 3594–3657.
[7] H. Chen, M. Ikeda-Saito, S. Shaik, *J. Am. Chem. Soc.* **2008**, *130*, 14778–14790.
[8] M. Costas, M. P. Mehn, M. P. Jensen, L. Que, *Chem. Rev.* **2004**, *104*, 939–986.
[9] E. G. Kovaleva, M. B. Neibergall, S. Chakrabarty, J. D. Lipscomb, *Acc. Chem. Res.* **2007**, *40*, 475–483.
[10] E. I. Solomon, D. E. Heppner, E. M. Johnston, J. W. Ginsbach, J. Cirera, M. Qayyum, M. T. Kieber-Emmons, C. H. Kjaergaard, R. G. Hadt, L. Tian, *Chem. Rev.* **2014**, *114*, 3659–3853.
[11] M. H. Stipanuk, C. R. Simmons, P. Andrew Karplus, J. E. Dominy, *Amino Acids* **2011**, *41*, 91–102.
[12] J. P. T. Zaragoza, D. P. Goldberg, in *Metallobiology* (Eds.: M. Ikeda-Saito, E. Raven), Royal Society Of Chemistry, Cambridge, **2018**, pp. 1–36.
[13] A. T. Fiedler, A. A. Fischer, *JBIC J. Biol. Inorg. Chem.* **2017**, *22*, 407–424.
[14] K. Ray, F. F. Pfaff, B. Wang, W. Nam, *J. Am. Chem. Soc.* **2014**, *136*, 13942–13958.
[15] E. I. Solomon, P. Chen, M. Metz, S.-K. Lee, A. E. Palmer, *Angew. Chem. Int. Ed.* **2001**, *40*, 4570–4590.
[16] A. A. A. Emara, A. M. Ali, A. F. El-Asmy, E.-S. M. Ragab, *J. Saudi Chem. Soc.* **2014**, *18*, 762–773.
[17] J. Cho, R. Sarangi, W. Nam, *Acc. Chem. Res.* **2012**, *45*, 1321–1330.
[18] C.-L. Wong, J. A. Switzer, K. P. Balakrishnan, J. F. Endicott, *J. Am. Chem. Soc.* **1980**, *102*, 5511–5518.
[19] M. L. Bowers, F. C. Anson, *J. Electroanal. Chem. Interfacial Electrochem.* **1984**, *171*, 269–280.
[20] B. Battistella, L. Iffland-Mühlhaus, M. Schütze, B. Cula, U. Kuhlmann, H. Dau, P. Hildebrandt, T. Lohmiller, S. Mebs, U. Apfel, K. Ray, *Angew. Chem. Int. Ed.* **2022**, DOI 10.1002/anie.202214074.
[21] Y. Jo, J. Annaraj, M. S. Seo, Y.-M. Lee, S. Y. Kim, J. Cho, W. Nam, *J. Inorg. Biochem.* **2008**, *102*, 2155–2159.
[22] K. Mase, K. Ohkubo, S. Fukuzumi, *J. Am. Chem. Soc.* **2013**, *135*, 2800–2808.
[23] Y.-H. Wang, M. L. Pegis, J. M. Mayer, S. S. Stahl, *J. Am. Chem. Soc.* **2017**, *139*, 16458–16461.
[24] Y.-H. Wang, B. Mondal, S. S. Stahl, *ACS Catal.* **2020**, *10*, 12031–12039.
[25] T. Corona, S. K. Padamati, F. Acuña-Parés, C. Duboc, W. R. Browne, A. Company, *Chem. Commun.* **2017**, *53*, 11782–11785.
[26] J. F. Schlagintweit, P. J. Altmann, A. D. Böth, B. J. Hofmann, C. Jandl, C. Kaußler, L. Nguyen, R. M. Reich, A. Pöthig, F. E. Kühn, *Chem. Eur. J.* **2021**, *27*, 1311–1315.
[27] J. B. Gordon, A. C. Vilbert, M. A. Siegler, K. M. Lancaster, P. Moënne-Loccoz, D. P. Goldberg, *J. Am. Chem. Soc.* **2019**, *141*, 3641–3653.
[28] B. M. Hoffman, D. H. Petering, *Proc. Nat. Acad. Sci.* **1970**, *67*, 637–643.
[29] W. Zhang, W. Lai, R. Cao, *Chem. Rev.* **2017**, *117*, 3717–3797.
[30] K. Mase, S. Aoi, K. Ohkubo, S. Fukuzumi, *J. Porphyrins Phthalocyanines* **2016**, *20*, 935–949.
[31] R. A. Baglia, J. P. T. Zaragoza, D. P. Goldberg, *Chem. Rev.* **2017**, *117*, 13320–13352.
[32] J. H. Zagal, *Coord. Chem. Rev.* **1992**, *119*, 89–136.
[33] P. S. Miedema, M. M. van Schooneveld, R. Bogerd, T. C. R. Rocha, M. Hävecker, A. Knop-Gericke, F. M. F. de Groot, *J. Phys. Chem. C* **2011**, *115*, 25422–25428.
[34] P. Vasudevan, Santosh, N. Mann, S. Tyagi, *Transition Met. Chem.* **1990**, *15*, 81–90.
[35] J. Premkumar, R. Ramaraj, *Radiat. Phys. Chem.* **1997**, *49*, 115–117.
[36] D. B. Rorabacher, J. F. Endicott, *Mechanistic Aspects of Inorganic Reactions*, American Chemical Society, Washington D. C., **1982**.
[37] W.-D. Wang, A. Bakac, J. H. Espenson, *Inorg. Chem.* **1995**, *34*, 4049–4056.
[38] J. Cho, R. Sarangi, H. Y. Kang, J. Y. Lee, M. Kubo, T. Ogura, E. I. Solomon, W. Nam, *J. Am. Chem. Soc.* **2010**, *132*, 16977–16986.
[39] W.-Y. Tcho, B. Wang, Y.-M. Lee, K.-B. Cho, J. Shearer, W. Nam, *Dalton Trans.* **2016**, *45*, 14511–14515.
[40] C.-C. Wang, H.-C. Chang, Y.-C. Lai, H. Fang, C.-C. Li, H.-K. Hsu, Z.-Y. Li, T.-S. Lin, T.-S. Kuo, F. Neese, S. Ye, Y.-W. Chiang, M.-L. Tsai, W.-F. Liaw, W.-Z. Lee, *J. Am. Chem. Soc.* **2016**, *138*, 14186–14189.
[41] P. Gerschel, K. Warm, E. R. Farquhar, U. Englert, M. L. Reback, D. Siegmund, K. Ray, U.-P. Apfel, *Dalton Trans.* **2019**, DOI 10.1039/C8DT04740E.
[42] L. Iffland, D. Siegmund, U. Apfel, *Z. Anorg. Allg. Chem.* **2020**, *646*, 746–753.
[43] P. Gerschel, B. Battistella, D. Siegmund, K. Ray, U.-P. Apfel, *Organometallics* **2020**, *39*, 1497–1510.
[44] P. Gerschel, A. L. Cordes, S. Bimmermann, D. Siegmund, N. Metzler-Nolte, U. Apfel, *Z. Anorg. Allg. Chem.* **2021**, *647*, 968–977.
[45] P. Zanello, R. Seeber, A. Cinquantini, G.-A. Mazzocchin, L. Fabbrizzi, *J. Chem. Soc. Dalton Trans.* **1982**, 893.
[46] T. L. Walker, S. Mula, W. Malasi, J. T. Engle, C. J. Ziegler, A. van der Est, J. Modarelli, M. J. Taschner, *Dalton Trans.* **2015**, *44*, 20200–20206.
[47] L. Siegfried, T. A. Kaden, *Helv. Chim. Acta* **1984**, *67*, 29–38.
[48] I. Monte Pérez, X. Engelmann, Y.-M. Lee, M. Yoo, E. Kumaran, E. R. Farquhar, E. Bill, J. England, W. Nam, M. Swart, K. Ray, *Angew. Chem. Int. Ed.* **2017**, *56*, 14384–14388.
[49] R. W. Hay, B. Kinsman, C. I. Smith, *Polyhedron* **1995**, *14*, 1245–1249.
[50] L. Fabbrizzi, A. Poggi, P. Zanello, *J. Chem. Soc. Dalton Trans.* **1983**, 2191.
[51] R. Bembi, R. Singh, S. V. Singh, *Transition Met. Chem.* **1991**, *16*, 200–203.
[52] J. F. Endicott, J. Lilie, J. M. Kuszaj, B. S. Ramaswamy, W. G. Schmonsees, M. G. Simic, M. D. Glick, D. P. Rillema, *J. Am. Chem. Soc.* **1977**, *99*, 429–439.
[53] D. F. Evans, *J. Chem. Soc. Resumed* **1959**, 2003.
[54] R. S. Drago, *Physical Methods for Chemists*, Saunders College Publishing, **1992**.
[55] G. L. Miessler, P. J. Fischer, D. A. Tarr, *Inorganic Chemistry*, Pearson, Boston, **2014**.
[56] JoVe Science Education Database. Anorganische Chemie. The Evans Method. JoVe, Cambridge, MA, **2022**.
[57] Deposition Numbers 2278389 (for **Co{i-N4}**) and 2278388 (for $Co_2(O_2)\{i\text{-}N_4\}_2$) contain the supplementary crystallographic data for this paper. These data are provided free of charge by the joint Cambridge Crystallographic Data Centre and Fachinformationszentrum Karlsruhe Access Structures service.
[58] S. Matsuoka, K. Yamamoto, T. Ogata, M. Kusaba, N. Nakashima, E. Fujita, S. Yanagida, *J. Am. Chem. Soc.* **1993**, *115*, 601–609.
[59] I. Monte-Pérez, S. Kundu, A. Chandra, K. E. Craigo, P. Chernev, U. Kuhlmann, H. Dau, P. Hildebrandt, C. Greco, C. Van Stappen, N. Lehnert, K. Ray, *J. Am. Chem. Soc.* **2017**, *139*, 15033–15042.
[60] Y. Tanabe, K. Nakajima, Y. Nishibayashi, *Chem. Eur. J.* **2018**, *24*, 18618–18622.
[61] A. Paul, R. Borrelli, H. Bouyanfif, S. Gottis, F. Sauvage, *ACS Omega* **2019**, *4*, 14780–14789.
[62] J. P. Hurvois, C. Moinet, *J. Organomet. Chem.* **2005**, *690*, 1829–1839.
[63] B. Su, I. Hatay, P. Y. Ge, M. Mendez, C. Corminboeuf, Z. Samec, M. Ersoz, H. H. Girault, *Chem. Commun.* **2010**, *46*, 2918.
[64] C. Franco, J. Olmsted III, *Talanta* **1990**, *37*, 905–909.
[65] M. L. Pegis, B. A. McKeown, N. Kumar, K. Lang, D. J. Wasylenko, X. P. Zhang, S. Raugei, J. M. Mayer, *ACS Cent. Sci.* **2016**, *2*, 850–856.
[66] A. M. Appel, M. L. Helm, *ACS Catal.* **2014**, *4*, 630–633.

[67] A. A. Fischer, S. V. Lindeman, A. T. Fiedler, *Dalton Trans.* **2017**, *46*, 13229–13241.
[68] M. J. Baldwin, P. K. Ross, J. E. Pate, Z. Tyeklar, K. D. Karlin, E. I. Solomon, *J. Am. Chem. Soc.* **1991**, *113*, 8671–8679.
[69] M. Suzuki, *Acc. Chem. Res.* **2007**, *40*, 609–617.
[70] J. D. Ortego, M. Seymour, *Polyhedron* **1982**, *1*, 21–30.
[71] Y. Le Mest, C. Inisan, A. Laouénan, M. L'Her, J. Talarmin, M. El Khalifa, J.-Y. Saillard, *J. Am. Chem. Soc.* **1997**, *119*, 6095–6106.
[72] A. Panja, *Dalton Trans.* **2014**, *43*, 7760.
[73] L. Nurdin, D. M. Spasyuk, L. Fairburn, W. E. Piers, L. Maron, *J. Am. Chem. Soc.* **2018**, *140*, 16094–16105.
[74] S. Schmidt, F. W. Heinemann, A. Grohmann, *Eur. J. Inorg. Chem.* **2000**, *2000*, 1657–1667.
[75] B. Shin, K. D. Sutherlin, T. Ohta, T. Ogura, E. I. Solomon, J. Cho, *Inorg. Chem.* **2016**, *55*, 12391–12399.
[76] J. J. Warren, T. A. Tronic, J. M. Mayer, *Chem. Rev.* **2010**, *110*, 6961–7001.
[77] A. Yadav, P. Mathur, *Inorg. Chim. Acta* **2015**, *435*, 206–214.
[78] P. Paul, R. D. Bolskar, A. M. Clark, C. A. Reed, *Chem. Commun.* **2000**, 1229–1230.
[79] X.-S. Xue, P. Ji, B. Zhou, J.-P. Cheng, *Chem. Rev.* **2017**, *117*, 8622–8648.
[80] A. Chandra, M. Ansari, I. Monte-Pérez, S. Kundu, G. Rajaraman, K. Ray, *Angew. Chem. Int. Ed.* **2021**, *60*, 14954–14959.
[81] J. Leonard, B. Lygo, G. Procter, J. Leonard, *Praxis der organischen Chemie: ein Handbuch*, VCH, Weinheim, **1996**.
[82] S. Stoll, A. Schweiger, *J. Magn. Reson.* **2006**, *178*, 42–55.
[83] R. D. Mair, A. J. Graupner, *Anal. Chem.* **1964**, *36*, 194–204.
[84] S. Fukuzumi, S. Kuroda, T. Tanaka, *J. Am. Chem. Soc.* **1985**, *107*, 3020–3027.
[85] D. J. Wasylenko, C. Rodríguez, M. L. Pegis, J. M. Mayer, *J. Am. Chem. Soc.* **2014**, *136*, 12544–12547.
[86] J. A. S. Roberts, R. M. Bullock, *Inorg. Chem.* **2013**, *52*, 3823–3835.
[87] G. M. Sheldrick, *Acta Crystallogr. Sect. A* **2008**, *64*, 112–122.
[88] G. M. Sheldrick, *Acta Crystallogr. Sect. Found. Adv.* **2015**, *71*, 3–8.
[89] G. M. Sheldrick, *Acta Crystallogr. Sect. C* **2015**, *71*, 3–8.
[90] O. V. Dolomanov, L. J. Bourhis, R. J. Gildea, J. A. K. Howard, H. Puschmann, *J. Appl. Crystallogr.* **2009**, *42*, 339–341.

Manuscript received: July 3, 2023
Revised manuscript received: August 1, 2023
Accepted manuscript online: August 2, 2023
Version of record online: August 29, 2023